Ocean Engineering 194 (2019) 106653

Contents lists available at ScienceDirect

Ocean Engineering

journal homepage: www.elsevier.com/locate/oceaneng

Numerical analysis of local and global responses of an offshore fish farm subjected to ship impacts

Zhaolong Yu [a,b,*], Jørgen Amdahl [a,b], David Kristiansen [c], Pål Takle Bore [a,b]

[a] Department of Marine Technology, Norwegian University of Science and Technology (NTNU), Norway
[b] Center for Autonomous Marine Operations and Systems (AMOS), Norwegian University of Science and Technology (NTNU), Norway
[c] SINTEF Ocean, Norway

ARTICLE INFO

Keywords:
Offshore fish farm
Ship collision
Coupled simulation
Local and global analysis
Structural damage

ABSTRACT

Due to limited nearshore areas and great impact to local ecosystems, the aquaculture industry is moving the fish farms into more exposed sea regions where the environmental conditions are much more severe. Like other offshore installations operating at sea, fish cages are also exposed to the risk of collisions from attendant or visiting vessels. This paper evaluates the structural strength of the world's first *offshore* fish farm operating in Norway subjected to supply vessel collisions by the use of nonlinear finite element simulations. The fish cage is a semi-submersible floating structure consisting of ring-stiffened columns connected by braces. A standard 7500-ton supply vessel is used as the striking vessel. Both local shell deformation analysis using LS-DYNA and beam deformation analysis using USFOS are carried out. In the local shell analysis, collision scenarios with both decoupled and coupled methods are simulated for several representative impact locations. The decoupled model adopts prescribed paths for ship motions, while in the coupled model, the ship motions are calculated based on hydrodynamic forces from linear potential theory as well as inertia and collision forces. In the global beam-column analysis in USFOS, the force-deformation curves of the supply vessel from local shell analysis are used as the input. The resulting damage and energy absorption are compared with those from local shell simulations. The results are discussed with respect to the impact resistance, energy absorption and structural damage.

1. Introduction

With the fish farming industry going into more exposed seas, the fish cages become larger and much more fish can be accommodated than ever before. However, harsher environmental loads and frequent aquaculture operations imply risk for accidental actions, such as ship collisions, where damage potential and possible consequences can be severe. Like other offshore installations e.g. jackets and jack-ups (Yu and Amdahl, 2018b; Le Sourne et al., 2016), submersible platforms and wind turbines (Biehl and Lehmann, 2006; Le Sourne et al., 2015), fish farms are exposed to the risk of collisions both from service vessels and merchant vessels on erroneous track. This may represent major threats to the safety and integrity of the fish farms. A major collision may cause extensive structural damage, and in extreme cases, the fish farm may collapse completely with fish escape as a result. Escape of farmed fish will cause major economic losses for the fish farming company and is considered to have negative impact on the wild stocks. More seriously, a collision event may also represent a safety threat for the personnel both on the ship and the fish farm. Hence, this should be avoided by either proper safety measures to reduce the likelihood of collision, by direct design or favorably by a combination. Design aspects of accidental loads from ship collisions are, however, not included in the present Norwegian technical standard for the design of fish farms (Standard-Norway-NS9415, 2009).

In addition to resisting the direct actions during collision, the damaged structure should maintain sufficient residual strength so that it can resist operational and environmental loads before it can be repaired. Realistic estimates of the environmental load levels at a given site and structural condition rely on adequate descriptions of the marine environment, including the exposure to wind, waves and current.

Ship collisions have been considered for decades in the offshore industry. In the design against ship collision actions, the kinetic energy of the vessel is determined by a risk assessment. The design practice in the North Sea that has been used for decades, was to consider impact from a supply vessel of 5000 tons, with a kinetic energy of 11 MJ for bow or stern impact and 14 MJ for sideway impact considering hydrodynamic

* Corresponding author. Department of Marine Technology, Norwegian University of Science and Technology (NTNU), Norway.
E-mail address: zhaolong.yu@ntnu.no (Z. Yu).

https://doi.org/10.1016/j.oceaneng.2019.106653
Received 29 April 2019; Received in revised form 20 September 2019; Accepted 26 October 2019
Available online 6 November 2019

Fig. 1. Illustration of the ocean farming concept '*OCEAN FARM 1*', illustration by Global Maritime.

Table 1
Principal dimensions of the striking vessel.

Displacement	7500 tons
Length	90 m
Breadth	18.8 m
Depth	7.6 m
Draft	6.2 m

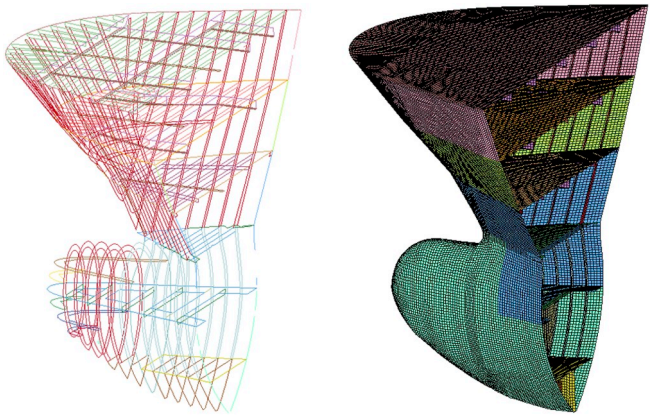

Fig. 2. The FE model of the bulbous bow.

effects. Over the years, the experienced collision energy has increased significantly due to increased ship sizes and impact velocities according to Kvitrud (2011), who summarized collision accidents in Norway in the period 2001–2010. In the latest version NORSOK-N003 (2017), displacements of the design supply vessel has increased to 6500–10 000 tons and the design impact velocities has increased to 3 m/s for head-on collisions and 2 m/s for side collisions (Moan et al., 2017). This yields a significantly larger design energy of about 50 MJ for head-on collisions. The NORSOK standards are developed for offshore structures used for oil and gas production, but standard collision actions for offshore fish farm has not been established. The intention of this work is to investigate the collision resistance and permanent damage of a selected fish farm as a function of the collision energy. No comparison is made with acceptance criteria as they have generally not been established, but possible evaluation criteria are discussed with the simulation results. It is emphasized that structural damage is investigated only; penetration of the net may occur for small impact energies, and the potential of fish escape can be large, even if integrity of the structure is not put in jeopardy.

The fish cage structure analyzed is the ocean farming concept '*Ocean Farm 1*' designed by Global Maritime, and it is considered the world's first *offshore* fish farm. Based on world-class Norwegian aquaculture and offshore technology, *Ocean Farm 1* aspires to address central issues related to sustainable growth in the aquaculture industry. The idea behind the Ocean Farming concept is to introduce a design robust enough to be safely installed and operated at exposed coastal sites. Instead of a traditional 'gravity' type cage, using a flexible floating collar and a weight system to support the net, it consists of a rigid frame supporting the net and a superstructure/wheelhouse containing living quarters and rig controls. To avoid drifting off, the structure is kept in place by eight mooring lines (Bore and Amdahl, 2017). An illustration of the concept is seen in Fig. 1. We emphasize that the dimensions used in the studies differ slightly from real dimensions of *Ocean Farm 1*.

The fish farm is a tubular structure consisting of braces and ring stiffened tubes. Many studies have been carried out on the impact response of tubular structures. Recent experimental studies on the indentation of tubular members or stiffened tubes are reported in Cerik et al. (2015), Qu et al. (2017), Firouzsalari et al. (2019), and Zhu et al. (2017). Empirical and analytical solutions to the indentation response of tubes were given in Wierzbicki and Suh (1988) and Amdahl (1980) decades ago. Le Sourne et al. (2016) and Pire et al. (2018) further developed the analytical solutions to predict the response of offshore wind turbine jackets to ship impacts. The model consisted of analytical solutions for several characteristic deformation modes of tubes, and has been verified to be of reasonable accuracy with numerical simulations. Numerical methods are also used to simulate the impact response of tubular structures, such as Le Sourne et al. (2015), Travanca and Hao (2015) and Wang et al. (2016). A comprehensive review on the impact response of tubular structures subjected to ship impacts is given in Yu and Amdahl (2018b).

Numerical simulations are used in this paper. For practical reasons, the striking vessel selected is a 7500-ton offshore supply vessel, which is larger than typical fish harvesting vessels and well boats, but it is not out of range. Thus the analysis results are conservative with respect to safety considerations of the fish cage. In section 2, the fish cage model, the striking supply vessel model and the collision scenarios are described in detail. The analysis is split into two steps, i.e. local deformation in the vicinity of contact using LS-DYNA (Hallquist, 2007) and global response analysis of the structure using USFOS (Soreide et al., 1999). Sections 3 and 4 present the decoupled and coupled simulation results,

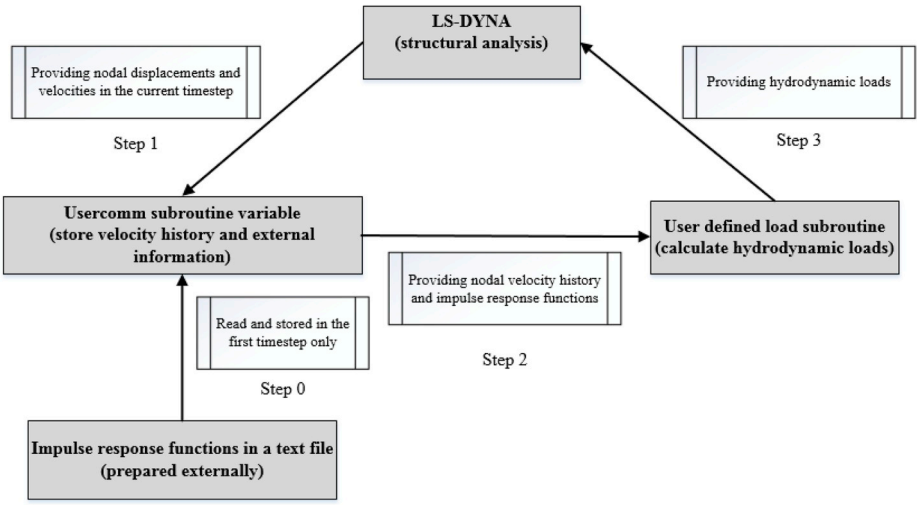

Fig. 3. Illustration of the coupling algorithm, from Yu et al. (2016).

respectively, with detailed shell modelling in LS-DYNA. Section 5 discusses results from global collision analysis using USFOS. Section 6 discusses design considerations and possible evaluation criteria. Section 7 concludes the paper.

2. Model descriptions

2.1. The striking supply vessel

A modern standard supply vessel bow is used in the study. The principal dimensions of the vessel are given in Table 1. The bow model is shown in Fig. 2. The element size is generally 120 mm. The plate thickness varies from 7 mm for the decks to 12.5 mm in the bulb. The stiffener spacing is approximately 600 mm, with ring stiffeners and breast hooks of approximately 250 × 15 mm in the bulb. The bulbous part is almost cylindrical and is relatively strong. The forecastle protrudes 1.2 m ahead of the bulb. Both decoupled and coupled simulations are carried out in the local structural analysis using LS-DYNA.

2.1.1. Decoupled ship collision simulation

In assessing the responses in ship collisions, the traditional approach is to decouple the problem into two parts: the external dynamics and the internal mechanics, as suggested by Minorsky (1958). The *external dynamics* models simplify the effect of fluid as constant added masses such that the whole collision system is un-damped and the principle of conservation of momentum and energy applies. This allows for a fast estimation of the dissipated energy and global motions after the collision. Examples of the *external dynamic* models are Pedersen and Zhang (1998) and Liu and Amdahl (2019). The lost energy will be dissipated by structural deformations and friction in the assessment of *internal mechanics* based on experiments, numerical simulations or analytical methods, (see e.g. (Ohtsubo et al., 1994; Paik, 2007; Marinatos and Samuelides, 2015; Cho and Lee, 2009), where the struck ship is normally fixed in space, and the striking ship moves along a prescribed path. The final penetration is obtained when the area under the force-penetration curve equals the energy loss resulting from the external dynamic calculations. The procedure is termed the "decoupled method", and has been widely used due to its simplicity and reasonable accuracy.

2.1.2. Coupled ship collision simulation

In contrast to the decoupled method, where ship motions are prescribed and hydrodynamic loads are much simplified, coupled models have been proposed to enable integrated ship collision simulations considering hydrodynamic loads and ship motions in more detail. Examples of the coupled models are provided by Petersen (1982), Tabri et al. (2010), Samuelides and Frieze (1989), Le Sourne et al. (2012), Pill and Tabri (2011) and Yu et al. (2016) with various simplifications. This paper adopts the advanced coupled model by proposed by Yu et al. (2016), which implements hydrodynamic loads based on linear potential flow theory into the nonlinear finite element code LS-DYNA by means of *user defined load subroutine*. It is assumed that before collision, propeller and rudder forces are in equilibrium with the hydrodynamic forces acting on the hull. Departure from this state due to a sudden change in the external forces causes a change in the hydrodynamic forces acting on the hull (Petersen, 1982). The governing motion equations are:

$$\sum_{k=1}^{6}\left[\left(M_{jk}+A_{jk}(\infty)\right)\ddot{\eta}_k+\int_0^t K_{jk}(t-\tau)\cdot[\dot{\eta}_k(\tau)-\dot{\eta}_k(t=0)]d\tau + C_{jk}\eta_k\right]=F_j(t)(j=1,2,\ldots,6) \tag{1}$$

where M_{jk} , $A_{jk}(\infty)$ andC_{jk} are components of the generalized ship mass matrix, the added mass matrix at infinite frequency and the restoring matrix of the ship. The index$j=1,\ldots,6$ represents surge, sway, heave, roll, pitch and yaw, respectively. $\dot{\eta}_k(t=0)$ is the velocity component of the striking ship in the k_{th} degree of freedom just before impact and $F_j(t)$ is the generalized collision force in the j_{th} degree of freedom. $\int_0^t K(t-\tau)\cdot\dot{\eta}(\tau)d\tau$ is the convolution integral connected with free-surface memory effects and $K_{jk}(t)$ is the so called impulse-response or retardation function connected with directions j and k. It provides a radiation load in j direction acting on the vessel at the actual time t as a consequence of an impulse speed in k direction experienced by the ship at a previous time instant t-τ. $K_{jk}(t)$ is given alternatively by:

$$K_{jk}(t)=\frac{2}{\pi}\int_0^\infty B_{jk}(\omega)\cos\,\omega t d\omega=\frac{2}{\pi}\int_0^\infty\left(A_{jk}(\infty)-A_{jk}(\omega)\right)\omega\,\sin\,\omega t d\omega \tag{2}$$

$A_{jk}(\omega)$ and $B_{jk}(\omega)$ are the frequency-dependent added mass and linear wave-radiation damping, respectively.

The coupling between nonlinear FEA structural solver and the linear hydrodynamic model is made possible by the user defined load subroutine (LOADUD). The coupling algorithm between structural and hydrodynamic solvers is shown in Fig. 3. During the simulation, LS-DYNA first passes information of nodal displacements, velocities and accelerations for the current timestep to the user subroutine. The selected node is the one at the ship center of gravity (COG). The velocity

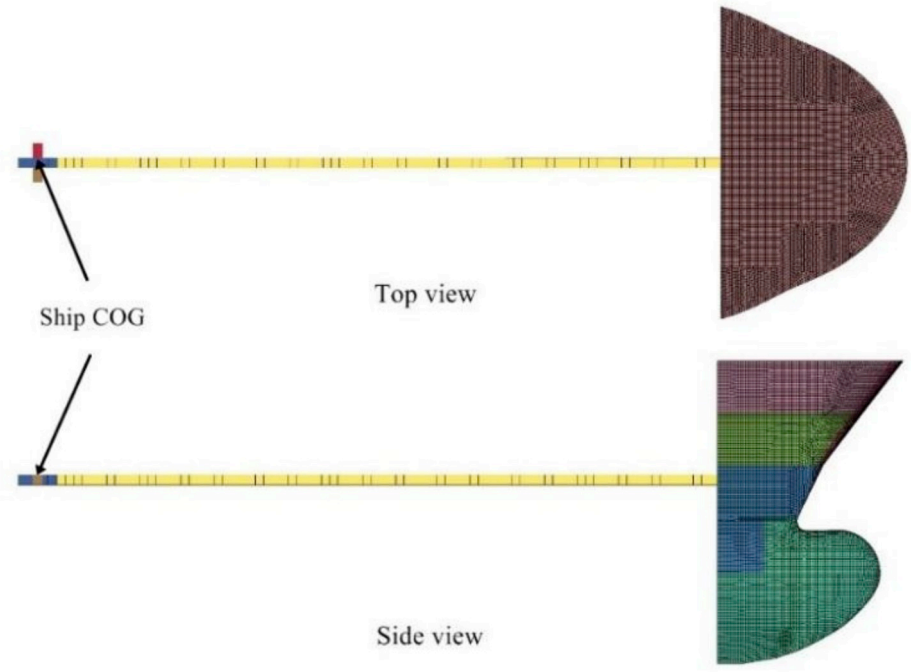

Fig. 4. The FE model of the striking ship.

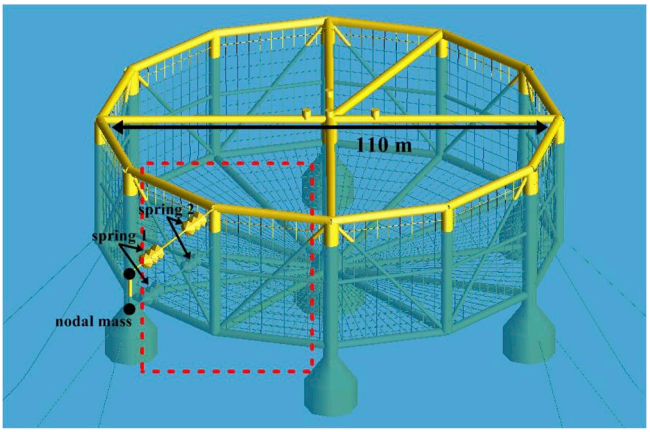

Fig. 5. The finite element model of the fish cage for USFOS collision analysis.

histories of COG are then stored through the user common subroutine. The time increment is typically in the order of 10^{-6} s in ship collision simulations. For maintaining efficiency without losing accuracy, the velocity histories are stored every 10^{-3} s. With the above information, the hydrodynamic loads can be calculated in the user load subroutine. The obtained hydrodynamic loads are applied on the ship COG, and LS-DYNA's structural solver then calculates structural deformation and ship motions, and provides information of ship motions for the next timestep. Verification has been carried out where the collision forces are extracted from LS-DYNA simulations and applied to the motion solver SIMO (Marintek, 2012), considering the resulting ship response based on linear potential flow theory. Motions measured from LS-DYNA simulation compared reasonably well with the SIMO results, demonstrating good accuracy of the implementation. More detailed description of the procedure is given in Yu et al. (2016).

In the coupled simulations, the ship's hull girder is represented by a long rigid beam from the bow back towards the center of gravity of the vessel; see Fig. 4. The rigid beam and the deformable ship bow are connected to a rigid shell plate at the rear of the bow model. The beam properties are calibrated to represent correctly the total mass and inertia of the ship with respect to the center of gravity, taking into account the contribution of the bow model. The 6DOF hydrodynamic forces and moments are applied as user-defined loads at the COG of the ship. Because the user defined load subroutine does not allow applying bending moments directly, the bending moments have to be transformed into force pairs. Therefore, several small rigid beams are created for applying bending moments in roll, pitch and yaw. The intersection of the beams is located at the center of gravity (see Fig. 4).

2.2. The fish cage model

The floating fish cage consists of many ring-stiffened tubes and columns that constitute a space frame. The cage is slack-moored at sea. The total displacement is approx. 16700 tons with a diameter of 110 m and the cage is designed to accommodate 1.5 million salmons. The finite element model of the whole fish cage is illustrated in Fig. 5, and is used for the global response analysis with USFOS. USFOS (Soreide et al., 1999) is a program aimed at ultimate strength and progressive collapse analysis of framed offshore structures. The basic idea of the program is to represent one physical element in the structure by one finite element, which is efficient but still preserves good accuracy. Nonlinear material properties are accounted for by means of yield hinge theory and interaction formulas for stress resultants. USFOS has been used by many researchers and designers in the analysis of framed structures such as jackets and jack-ups (Yu and Amdahl, 2018b) and floating bridges (Sha et al., 2019). In the global collision analysis with USFOS, the ship stiffness is modeled by two spring systems, representing stiffness of the ship stem on the upper layer and bulb stiffness on the lower layer. The two spring systems are rigidly connected by a rigid beam, and nodal masses are used to represent the ship mass including hydrodynamic added mass. It is important to allow the ship to detach from the fish cage at the end of impact. Therefore, a two-spring system is used in each layer as shown in Fig. 5. Spring 1 is the nonlinear spring that is defined by the force–deformation curve obtained from the local collision analysis in LS-DYNA with the detailed ship model. Spring 2 has an "infinite" stiffness in compression and zero stiffness in tension to facilitate separation. With the used mass-spring system, the interaction between the ship and

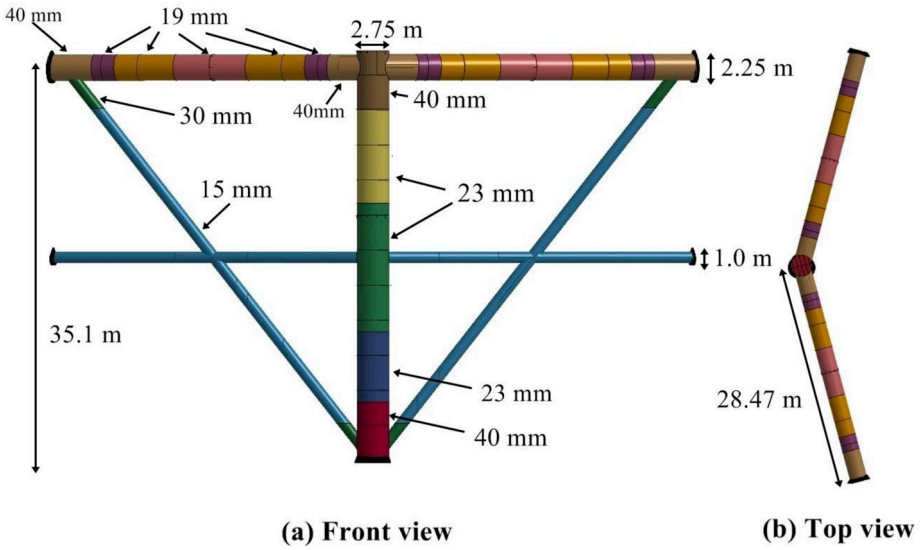

Fig. 6. Finite shell element sub-model for LS-DYNA local analysis.

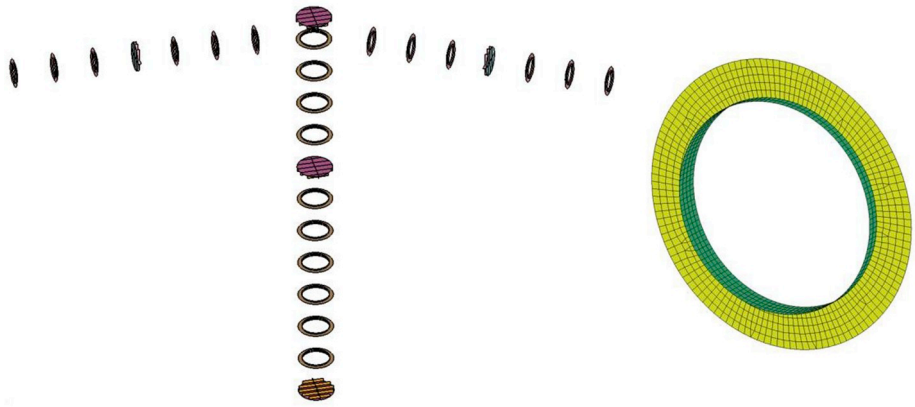

Fig. 7. Arrangement of ring stiffeners and the finite element model.

Table 2
Material properties for the ship and brace/leg models.

Material	Density (kg/m^3)	σ_y (Mpa)	E (Gpa)	K (Mpa)	n	$\varepsilon_{plateau}$	ε_n
supply vessel	7850	275	207	830	0.24	0.01	0.69
fish cage	7850	355	207	780	0.22	0.00	0.63

the fish cage can be accurately modeled.

For local strength assessment of the fish cage, a detailed shell finite element sub-model is made as shown in Fig. 6. The selected part is indicated by the dashed line in Fig. 5. The middle column is 35.1 m in height with a column diameter of 2.75 m. The column outer shell thickness varies from 23 mm to 40 mm. The columns are equipped with ring stiffeners T300 × 200 × 10 × 15, which are arranged every 3 m. The connecting transverse tube is 2.25 m in diameter and the tube thickness varies from 19 mm to 40 mm. Ring stiffeners with dimensions of T300 × 200 × 10 × 15 are arranged every 3.2 m. The arrangement of ring stiffeners of the fish cage is shown in Fig. 7.

The four-node Belytschko-Lin-Tsay shell element is used. The shell element size for the local cage model is in general 100 mm, which is typically adopted in ship collision analysis. This preserves good efficiency without losing accuracy. This shell element size is consistent with acceptable element size range, i.e. 5–10 times of the shell thickness, that gives adequate performance of fracture models with coarsely meshed shell elements (Storheim, 2016). More refined meshes are used for the ring stiffeners and stringers. Five elements are used for the stiffener web and four elements are used for the stiffener flange. This is considered sufficient to develop buckling modes (see Fig. 7). For simplicity, the ends of the column, the supporting tubes and the supporting braces, marked in black in Fig. 6, are fixed in all degrees of freedom. This boundary conditions are later discussed by comparison with global USFOS analysis.

2.3. Material modelling

When ship-structure interaction is accounted for, proper modelling of the material behavior is essential. This is because the relative strength of the striking and struck objects are very sensitive to material strength and fracture. A rupture of structures can easily turn the strong structure into the weak.

The steel material properties used for modelling the ship and the fish cage are given in Table 2. The power law hardening model is used to model plastic strain hardening for steel where the coefficients K and n are determined form the stress-strain curves for the material. A yield plateau is defined to delay the onset of hardening, and the plateau in the stress-strain curve of steel is observed in many uniaxial tensile tests, e.g. Noh et al. (2018). For the steel used in the fish cage, the plateau was specified to be zero, and this allowed use of the traditional power law

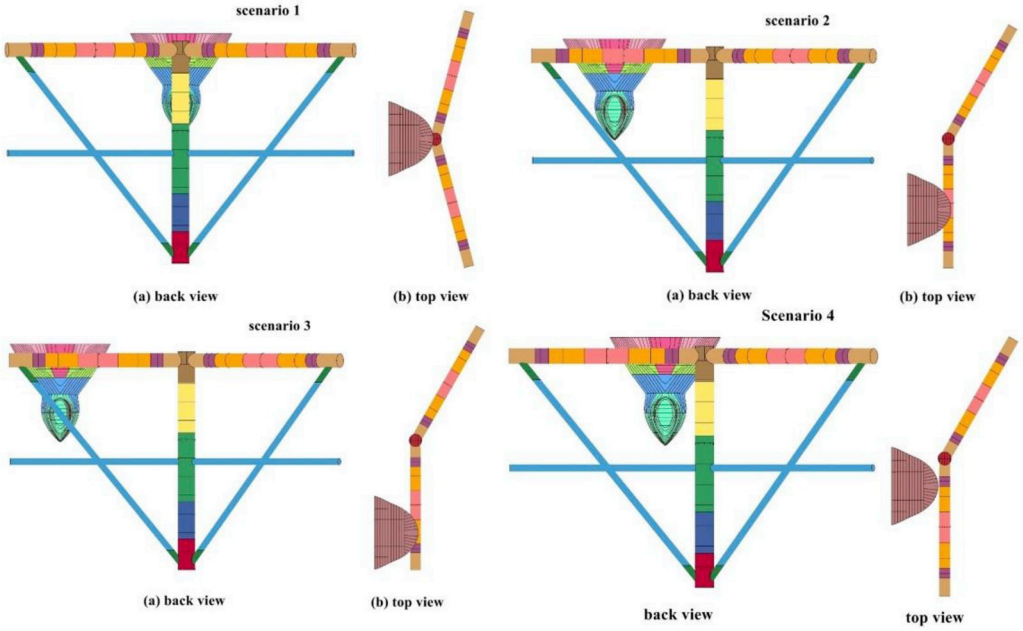

Fig. 8. The collision scenarios for decoupled simulations.

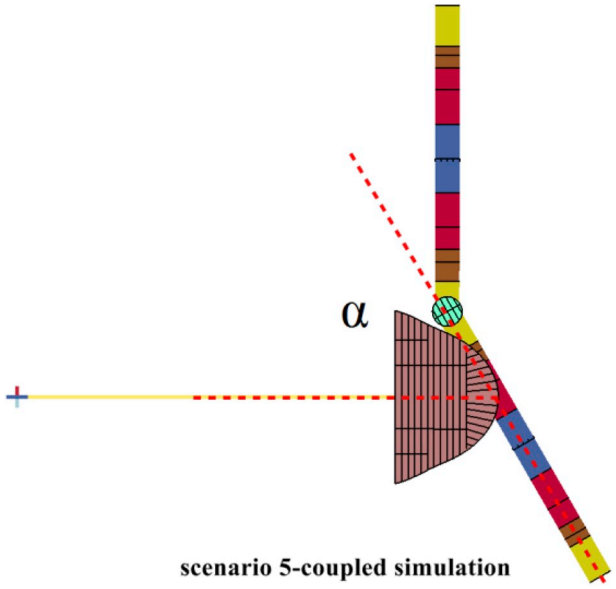

Fig. 9. The collision scenario for the coupled simulation.

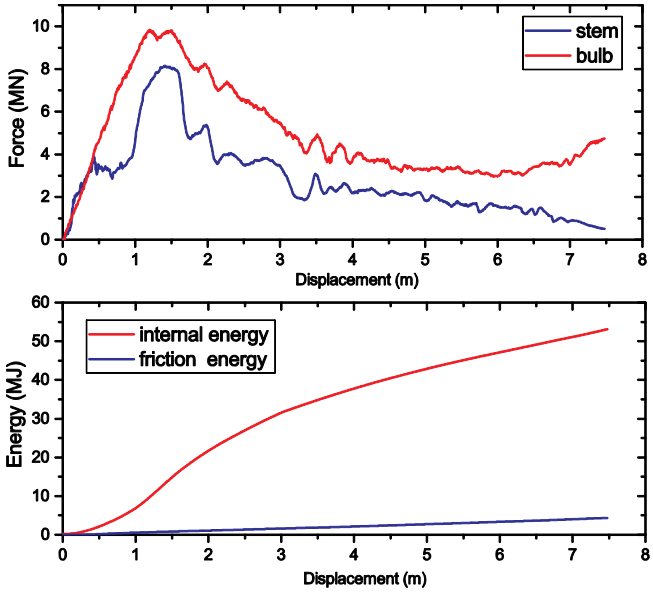

Fig. 10. Collision energy and resistance for collision scenario 1. The displacement is measured as displacement of the ship hull and includes deformations of the bow as well as the structure.

model. For the mild steel that is typically used in supply vessels, the guaranteed minimum yield strength is 235 MPa. However, there is no strict requirement for the upper bound of the material strength. As the crushing bow represents a "load" in this context, the material is assumed to behave as a NV DW27 material with a yield strength of 275 MPa and significant strain hardening to simulate a more realistic yield strength (Storheim and Amdahl, 2014). This is in accordance with the design principles outlined in DNV RP C208 standard (DNV-RP-C208, 2016).

The state-of-art Rice-Tracey-Cockcroft-Latham (RTCL) damage criteria (Tørnqvist, 2003) is used to model ductile fracture, which combines the model by Rice and Tracey (1969) for tension dominated damage and the model by Cockcroft and Latham (1968) for shear dominated damage. A cut-off value of $-1/3$ of the stress triaxiality $T = \frac{\sigma_1+\sigma_2+\sigma_3}{3\sigma_{eq}}$was introduced ($\sigma_i$is the i_{th} major principal stress, $\sigma_{eq}$is the von-Mises equivalent stress), below which the material is dominated by compression and no fracture will occur. The damage rate $\dot{D}$ is defined as:

$$\dot{D} = \begin{cases} 0 & \text{if } T < -1/3 \quad \text{(compression)} \\ \frac{\sigma_1}{\sigma_{eq}}\dot{\varepsilon}_{eq} & \text{if } -1/3 \le T < 1/3 \quad \text{(shear)} \\ \exp\left(\frac{3T-1}{2}\right)\dot{\varepsilon}_{eq} & \text{if } T \ge 1/3 \quad \text{(tension)} \end{cases} \tag{3}$$

where σ_1 is the major principal stress and $\dot{\varepsilon}_{eq}$ is the rate of equivalent plastic strain. An important feature with this criterion is that in uniaxial tension conditions (T = 1/3), the damage evolution$\dot{D}$is exactly matched by the rate of equivalent plastic strain$\dot{\varepsilon}_{eq}$. This is convenient with respect to calibration, because the critical damage most easily can be found from

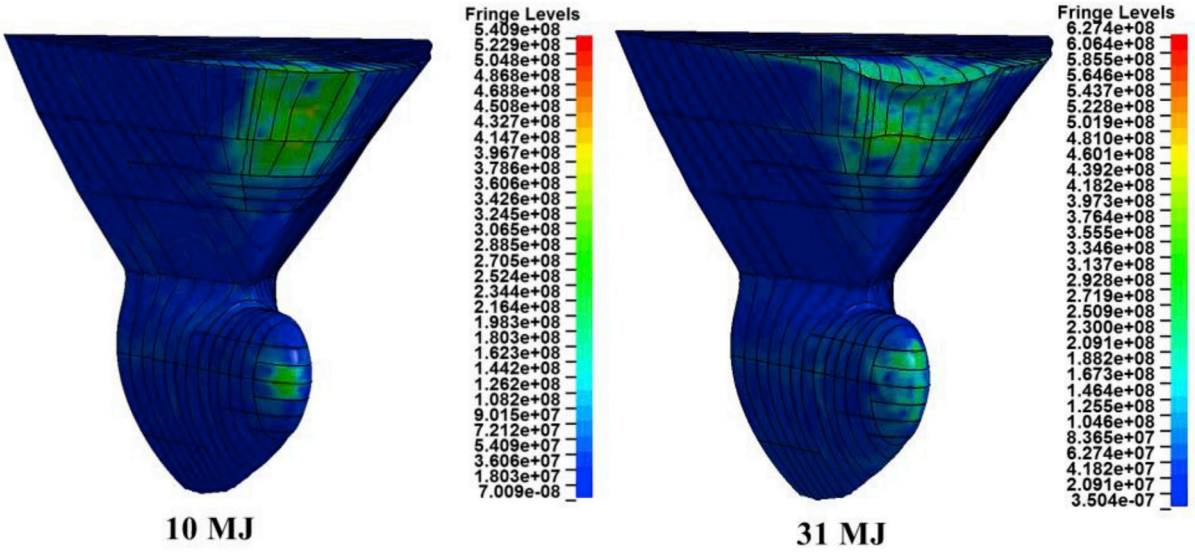

Fig. 11. The ship bow deformation after a total energy dissipation of 10 MJ and 31 MJ; (Scenario 1).

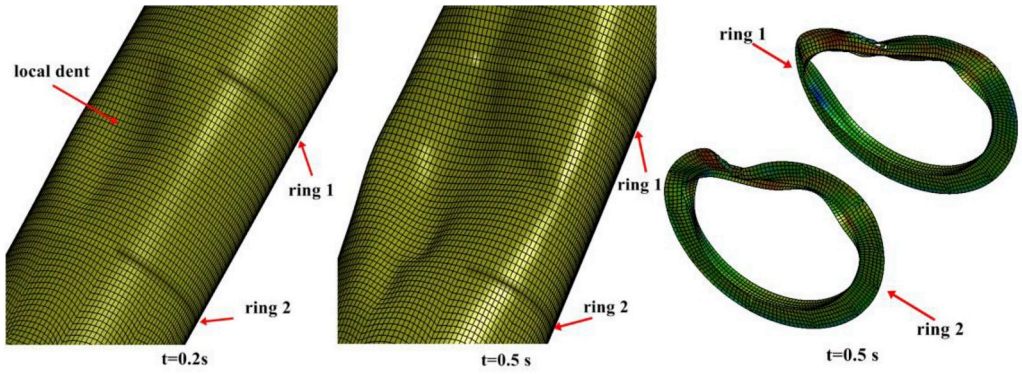

Fig. 12. Initial buckling of the fish cage structure at a displacement of 1.6 m (Scenario 1).

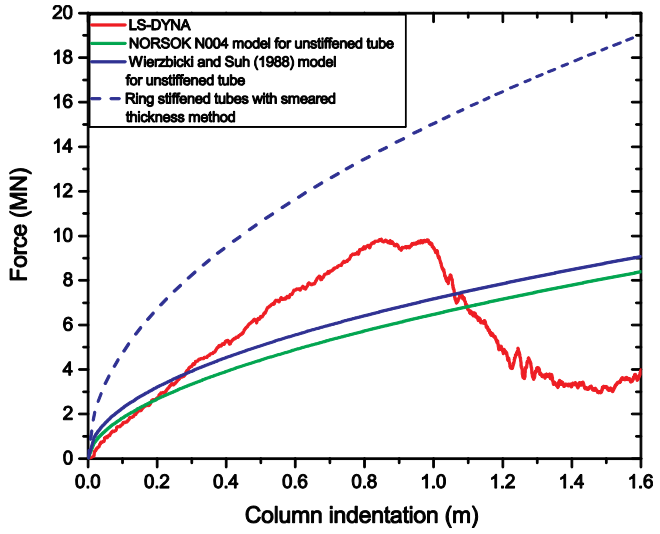

Fig. 13. Force-indentation curve from numerical simulations and from NORSOK N004; the indentation is calculated as the change of the diameter during collision. (Scenario 1).

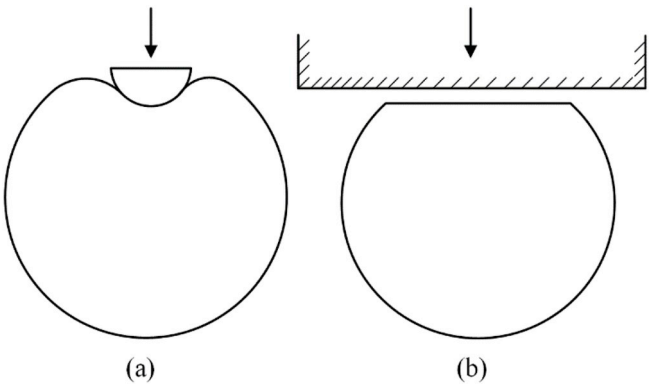

Fig. 14. Cross sections of ring stiffened columns subjected to lateral impact (Yu and Amdahl, 2018b).

uniaxial tensile tests. From this, a normalized damage criterion can be expressed as:

$$D_{normalized} = \frac{1}{\varepsilon_{cr}} \int \dot{D} dt \tag{4}$$

where, $\varepsilon_{cr}$is the critical equivalent plastic strain in uniaxial tension. Fracture is triggered when the normalized accumulated damage

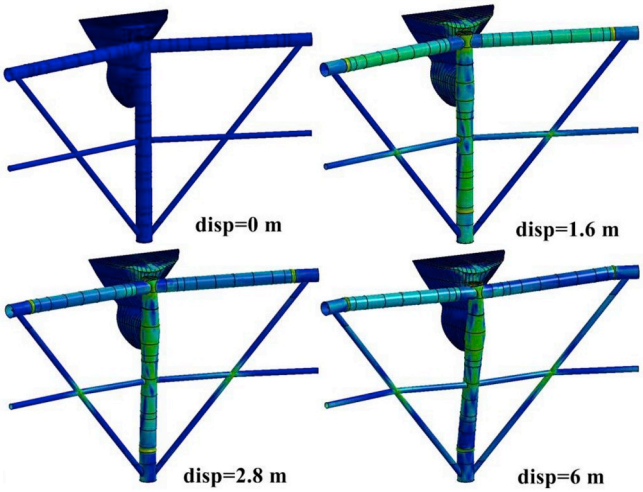

Fig. 15. Structural deformations at different total displacements (Scenario 1).

$D_{normalized}$ reaches 1.

To account for the mesh size effect, ε_{cr} is mesh scaled in accordance with the relationship:

$$\varepsilon_{cr} = n + (\varepsilon_n - n)\frac{t_e}{l_e} \tag{5}$$

where ε_n is the failure strain in the simulation of uniaxial tension tests with a mesh size of $l_e = t_e$ and n is the power law exponent.

The adopted solver for the RTCL fracture criterion was implemented by Alsos et al. (2009) and Storheim et al. (2015) and has been calibrated and validated to be of good accuracy with plate tearing tests by Simonsen and Törnqvist (2004), indentation experiments of double sided shell structure by Tautz et al. (2013) and large scale collision tests by Peschmann (2001).

2.4. Collision scenarios for local structural analysis

2.4.1. Decoupled simulations

Four collision scenarios are analyzed for the decoupled simulations, as shown in Fig. 8.

Scenario 1: Bow collision with the column
Scenario 2: Bow collision with the middle of the transverse supporting tube
Scenario 3: Bow collision with one quarter span of the transverse supporting tube and diagonal braces for scenarios
Scenario 4: Bow collision with the other quarter span of the transverse supporting tube

The relative position of the ship and the fish cage is adjusted according to the operational draft of both structures. The striking ship is assumed to move with a prescribed velocity of 3 m/s. The penalty based contact algorithms are used to model the contact between the vessel and the fish cage, and the internal contact in the ship and the fish cage itself. A friction coefficient of 0.3 is assumed for all the contacts.

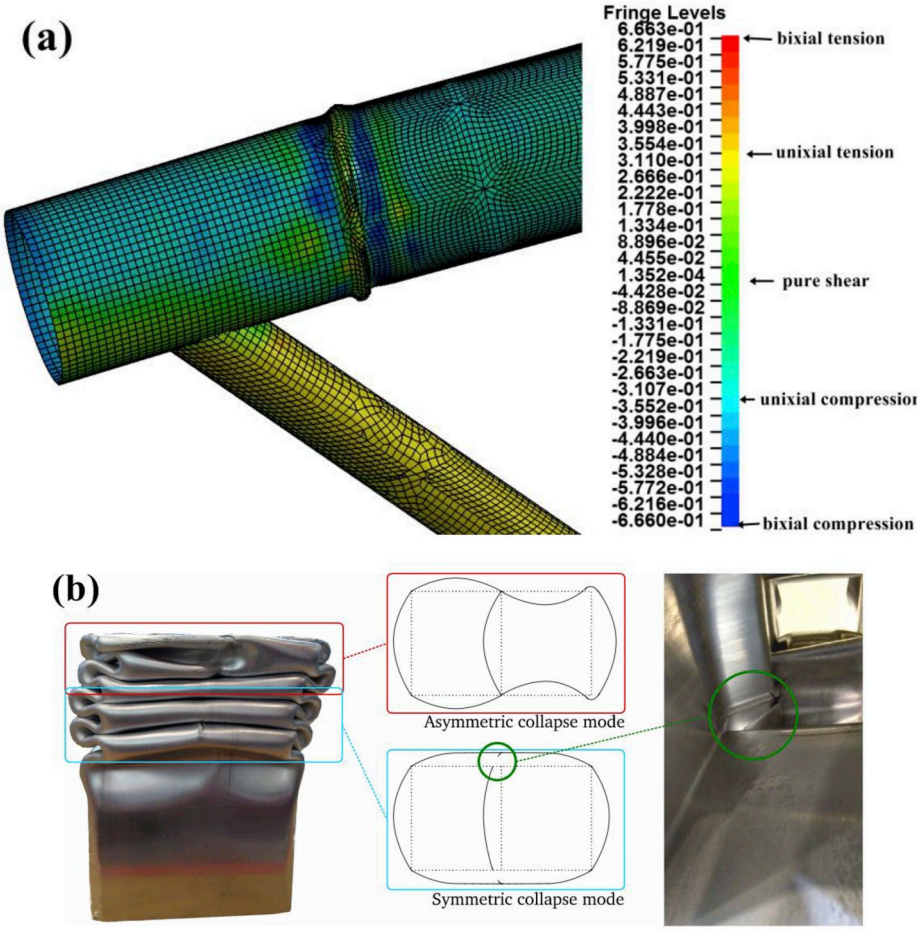

Fig. 16. (a) Stress triaxiality distribution at the left end of the transverse supporting tube at a displacement of 2.8 m; (b) deformation and fracture of square tubes under axial compression; from Costas et al. (2019).

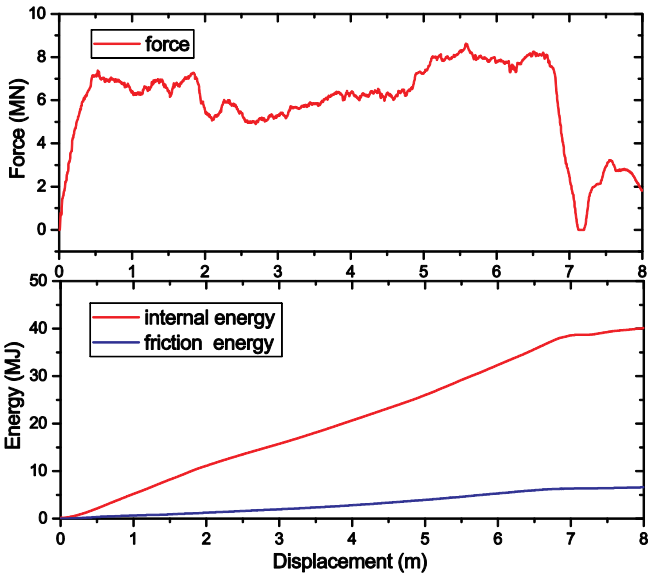

Fig. 17. Collision energy and resistance for scenario 2.

2.4.2. Coupled simulations

A scenario 5 is established for the coupled collision analysis in Fig. 9. The collision angle is $\alpha = 60°$. The ends of the column, the supporting tubes and the supporting braces are fixed against all degrees of freedom motions. The striking ship is given an initial velocity of 3 m/s in accordance with the latest version of NORSOK-N003 (2017) rather than prescribed trajectories in decoupled simulations.

3. Local decoupled collision simulation results

3.1. Collision scenario 1: bow impact on the middle column

In scenario 1, the supply vessel collides with the main column as shown in Fig. 8. The resulting energy dissipation and collision resistance are shown in Fig. 10. A total energy of about 31 MJ is dissipated for a total ship displacement of 2.8 m, where fracture initiates. The total displacement of the ship equals the sum of the deformation and motion of the ship bow and the deformation of the cage.

The collision forces for the stem and bulb attain a peak after a displacement of 1.6 m and then drop drastically. The energy dissipation before the drop is around 16.3 MJ. Up to this point, the column deformation is generally local. The column top with a stiffened plate is quite strong and is able to crush the ship stem as shown in Fig. 11. At the lower contact point, the ship bulb is strong and crushes the column causing only minor bulb deformation while the column undergoes significant local denting; see Fig. 12.

Design formulations for the indentation resistance of unstiffened tubes are given in NORSOK-N004 (2004). The model takes the following form:

$$R / R_c = \left(22 + 1.2\frac{B}{D}\right)\left(\frac{w_d}{D}\right)^{\frac{1.925}{3.5+\frac{B}{D}}}\cdot\sqrt{\frac{4}{3}\left(1-\frac{1}{4}\left[1-\frac{N}{N_p}\right]^3\right)} \tag{6}$$

where, $R$is the indentation resistance,σ_y is the material yield stress, B is the contact width, D is the tube dimeter and t is the wall thickness. $R_c = \frac{1}{4}\sigma_y t^2\sqrt{\frac{D}{t}}$ is a characteristic resistance of the tube against local denting. N is the axial force applied on the tube and $N_p$is fully plastic axial yield force of the cross section.

Wierzbicki and Suh (1988) derived a closed form solution for the indentation resistance of tubes under combined loading in the form of lateral indentation, bending moment and axial force. The problem was decoupled into bending and stretching of a series of unconnected rings and generators. The indentation resistance reads:

$$\frac{R}{R_c} = 16\sqrt{\frac{2\pi}{3}\frac{w_d}{D}}\cdot\sqrt{1-\frac{1}{4}\left(1-\frac{N}{N_p}\right)^3} \tag{7}$$

Fatt and Wierzbicki (1991) extended Wierzbicki and Suh (1988)'s model to consider indentation of ring stiffened columns by using the smeared thickness method. The equivalent thickness $t_{eq}$is found by equating the total bending moment over a characteristic length (equal to the spacing between stiffeners) of the stiffened shell to that of an unstiffened shell of assumed thickness. The resulting indentation resistance of ring-stiffened tubes is:

$$\frac{R}{R_c} = 16\frac{t_{eq}}{t}\sqrt{\frac{2\pi}{3}\frac{w_d}{D}}\cdot\sqrt{1-\frac{1}{4}\left(1-\frac{N}{N_p}\right)^3} \tag{8}$$

Fig. 13 compares the force-indentation curve from numerical simulations and from the analytical models. It shows that the NORSOK model and the Wierzbicki and Suh model for unstiffened tubes captured the development of resistance with indentation reasonably well in the initial stage. When the ring stiffeners get involved in the deformation and in the late stage when the brace starts global bending, the predicted resistance with unstiffened tube models becomes lower. With the

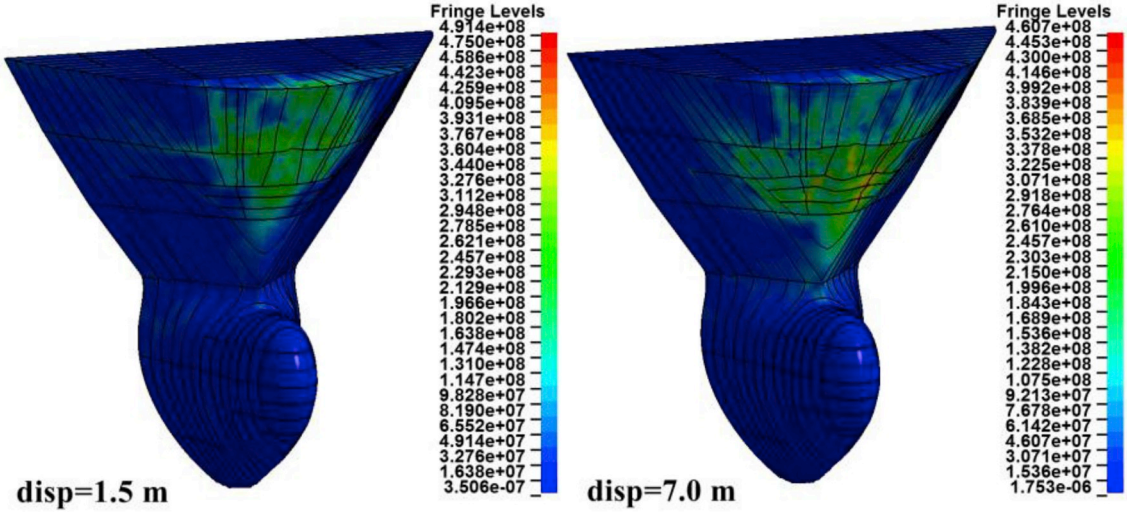

Fig. 18. Deformation of the ship bow (scenario 2).

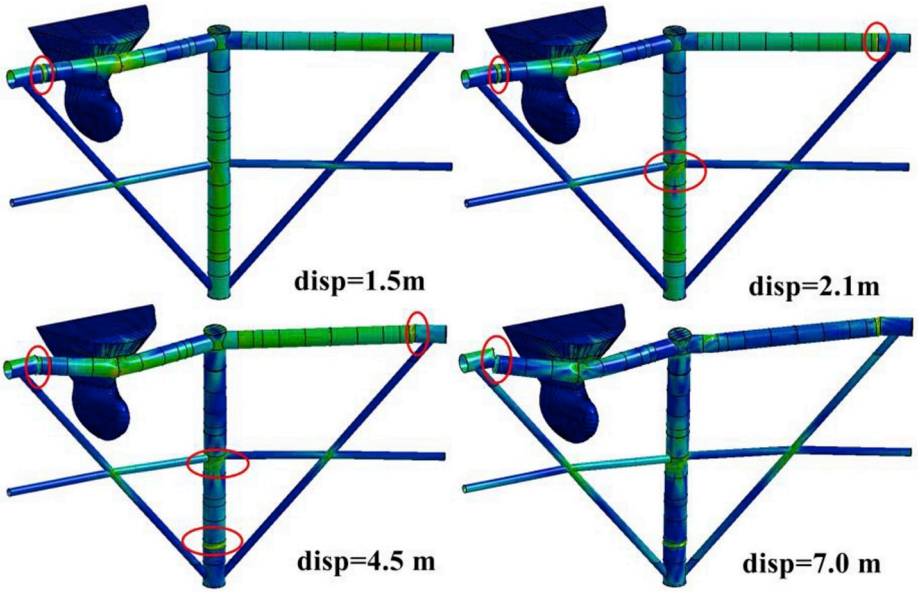

Fig. 19. Deformation of the fish cage at different total displacements (Scenario 2).

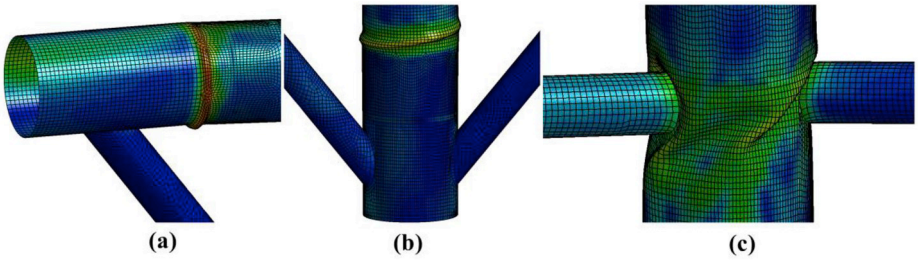

Fig. 20. Local buckling of tube cross sections at a displacement of (a) 2.1 m; (b) 4.5 m; (c) 4.5 m.

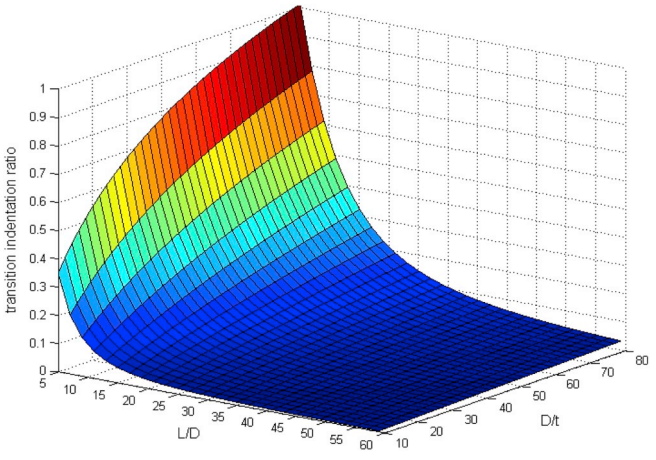

Fig. 21. Variations of transition indentation ratios from denting to bending with different L/D and D/t (Yu and Amdahl, 2018a).

smeared thickness method for ring stiffened tubes, the model predicts much higher resistance than that from numerical simulation. This is mainly because the bulb exerts a very concentrated action as shown in Fig. 14(a), while the used analytical models for dent formulations are based on a transverse, plane object as shown in Fig. 14(b). Anyway, the numerical simulation result falls within the analytical resistance curves for stiffened and unstiffened tube models.

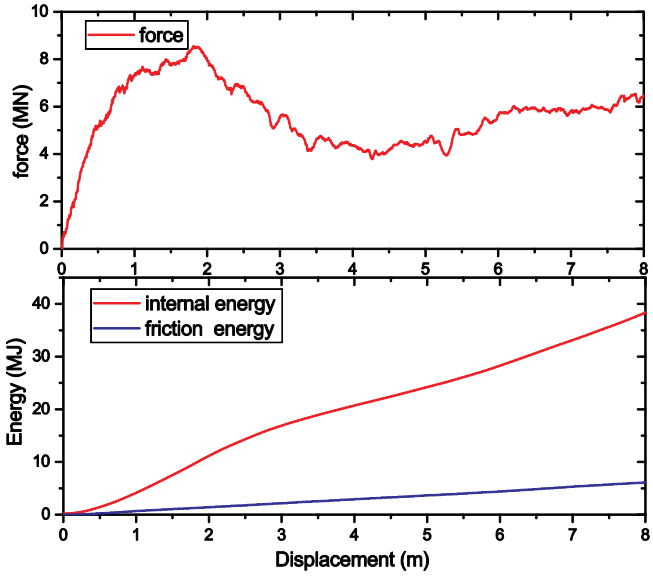

Fig. 22. Collision energy and resistance for scenario 4.

Global deformation starts with a sudden drop of forces due to initiation of local buckling, as shown in Fig. 15. This eases the contact between the ship stem and the top column plate. Considering the high diameter/thickness ratio (= 120), this is expected. According to ISO

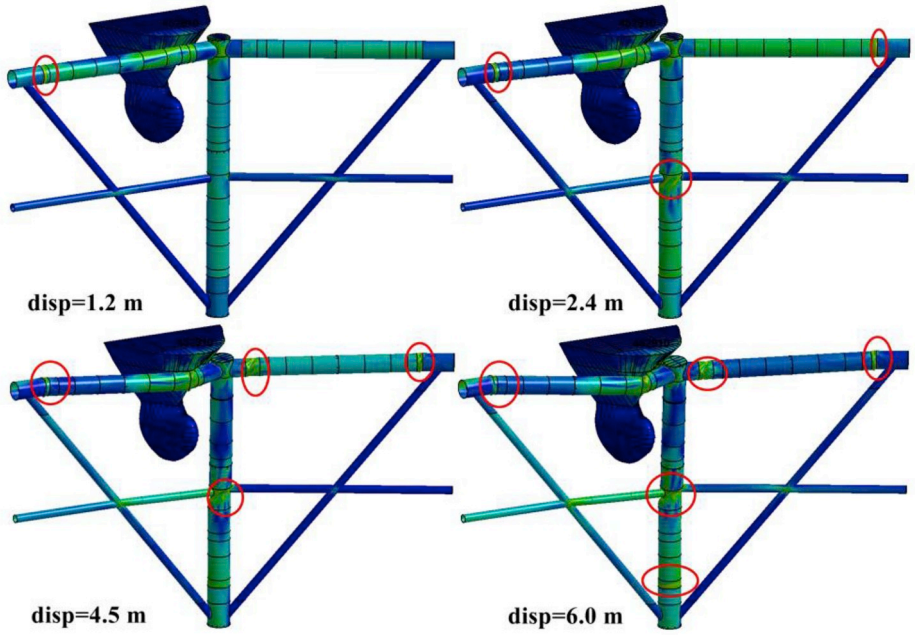

Fig. 23. Deformation of the fish cage for different dissipated energy levels (scenario 4).

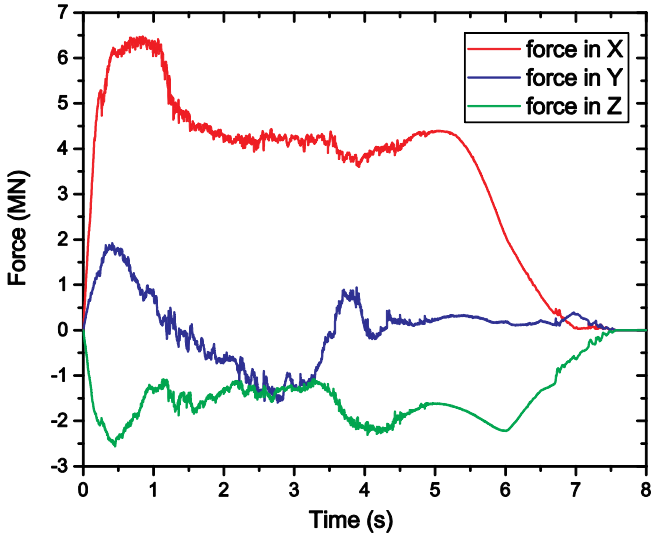

Fig. 24. The time variation of the collision forces (scenario 5).

19902 standard for fixed steel offshore structures, the ultimate bending moment capacity of the cross-section corresponds to first yield only, and the cross-section is thus not capable of developing a plastic hinge. Local buckling forms at the junction of shells where the thickness changes from 19 mm to 40 mm; The whole structure starts to deflect globally. As the local buckle develops, the bending moment and collision force drop. Deformation continues after initial buckling, and lateral column deflection increases significantly. For a total energy dissipation of 31 MJ corresponding to a displacement of 2.8 m, the left end of the transverse tube undergoes onset of fracture and the corresponding stress triaxiality distribution is shown in Fig. 16 (a). It is interesting to find that the tube is under compression globally, but this induces local buckling and material bulging. Fracture occurs due to the combined local bending and membrane loading caused by global compression loads. This is similar to the case of local fracture of square tubes under axial crushing; refer Fig. 16 (b) (Costas et al., 2019). Such fracture pattern does not propagate fast and considerable capacity is maintained after initial fracture.

3.2. Collision scenario 2: bow impact on the middle of the transverse tube

In collision scenario 2, the ship stem hits the middle of the transverse supporting tube. The collision resistance and the internal energy are plotted in Fig. 17. It shows that the structure can absorb about 8.2 MJ before initiation of fracture at a displacement of 1.5 m. This energy is significantly lower than the value in scenario 1. However, because fracture occurs due to progressive buckling as in scenario 1, the crack does not propagate fast and the structure still preserves considerable capacity. From the resistance and energy curves in Fig. 17, final collapse occurs at a total displacement of 7.0 m corresponding to a total energy of 40 MJ. Fig. 18 shows that the ship undergoes little damage during collision, and most of the energy (36 MJ) is dissipated through deformation of the cage.

Fig. 19 shows deformation of the fish cage at different total displacements. For a total displacement of 1.5 m, local buckling occurs at the shell connection, where the thickness shifts from 19 mm to 40 mm. As collision continues, additional buckling occurs in other places, including the transverse tube on the right side and the main column. The buckled cross section is shown in Fig. 20. Buckling at the intersection of the main column and the diagonal braces is induced by torsional moments.

3.3. Collision scenario 3 & 4: bow impact on the quarters of the transverse tube

In collision scenario 3, the ship crushes both the horizontal tube quarter close to the diagonal brace. A significant part of the energy is absorbed by membrane stretching of the braces. This effect may be exaggerated because of the fully fixed boundary conditions.

During collision, tubular braces/legs deform first by local indentation. Local denting continuously degrades the plastic bending capacity of the tube. When a certain indentation is reached, the brace starts to collapse as a beam forming a three-hinge mechanism. Upon further deformation, axial membrane forces will occur. In the design of such structures, one should be careful to rely on the membrane forces to dissipate too much energy because of the sensitivity to the axial flexibility of the boundaries (Yu and Amdahl, 2018b). For the studied fish cage, the diagonal brace of the fish cage has a thickness of 15 mm, a diameter of 1 m and a length of about 20 m. This gives a large length

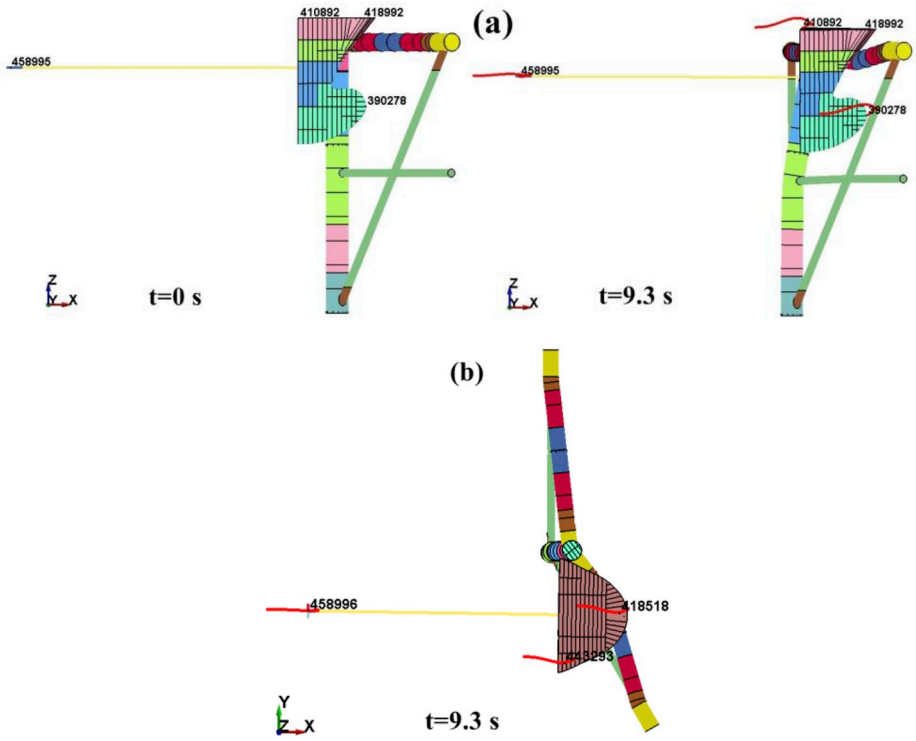

Fig. 25. Ship motions during the collision (a) side view (b) top view; the red lines indicate ship trajectories over time. (scenario 5). (For interpretation of the references to colour in this figure legend, the reader is referred to the Web version of this article.)

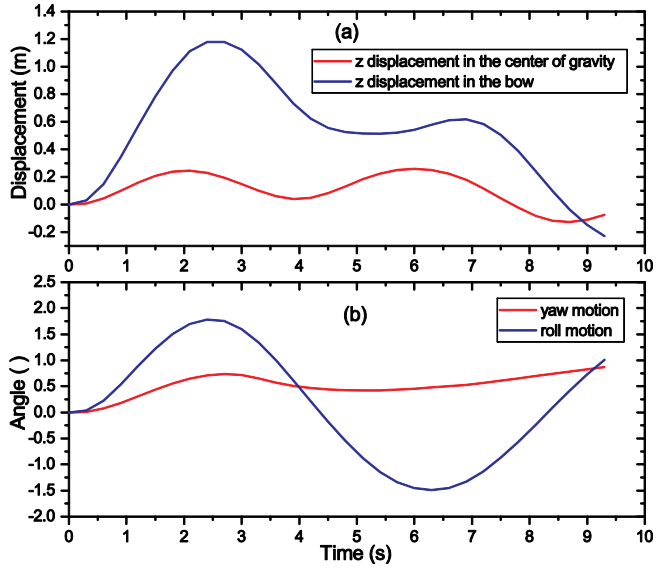

Fig. 26. (a) Vertical displacements at the center of gravity and the bow; (b) the yaw and roll motion with time (scenario 5).

over diameter ratio of 20 and a diameter over thickness ratio of 66.7. Based on the established transition ratio chart from denting to global bending by Yu and Amdahl (2018a) as shown in Fig. 21, the brace with given dimensions starts global bending immediately. In addition, the tube has a characteristic resistance for denting$R_c = \frac{1}{4}\sigma_y t^2\sqrt{\frac{D}{t}} = 0.16(\mathrm{MN})$, which is significantly lower than 1.4 MN recommended by the updated DNV-RP-C204 (2016) standard for maintaining cross sections compact. This implies that the tube cross section will be significantly dented and the dented cross section loses the capability to dissipate energy by bending. Consequently, the energy that can be dissipated by the braces through local denting and plastic hinges is quite limited, and the brace dissipates most energy through membrane stretching provided that the supporting columns acting as boundaries are strong enough against the pull-in$2\pi rt\sigma_y = 33.5(\mathrm{MN})$. This is far larger than the force level in Figs. 10 and 17. During design, it is often not credible to rely on membrane stretching to dissipate a significant amount of energy and are thus not discussed in detail.

In collision scenario 4, the ship crushes the other quarter of the upper transverse supporting tube away from the diagonal brace. The collision resistance and internal energy are shown in Fig. 22. Initial fracture occurs at a displacement of 2.4 m, corresponding to an energy dissipation of 14 MJ. As fracture occurs due to local bending and membrane loading caused by global compression loads, the crack does not propagate fast and considerable capacity remains. From Fig. 22, the structure can absorb around 40 MJ at a displacement of 8.0 m without complete collapse. However, such large displacements should be avoided in order not to penetrate into the cage, causing fish escape.

The deformation of the fish cage structure at different total displacements is shown in Fig. 23. When the ship moves 1.2 m into the fish cage structure, initial local buckling occurs on the left side of the transverse tube, corresponding to an energy dissipation of 5.5 MJ. As the collision continues, buckling occurs at several similar places as in scenario 2.

4. Local coupled collision simulation-scenario 5

Scenario 5 is simulated using the coupled solver, considering hydrodynamic loads and ship motions. The initial collision angle is 60°. The collision force components are plotted in Fig. 24. The collision lasts for about 7.5 s, which is relatively long and comparable to ship natural periods. All three force components are significant. Fig. 25 shows both side view and top view of ship motion trajectories at the bow and at the ship center of gravity. The temporal variation of the vertical displacement is plotted in Fig. 26(a). These plots show that the pitch and heave motions are significant. The ship bow moves a maximum of 1.15 m

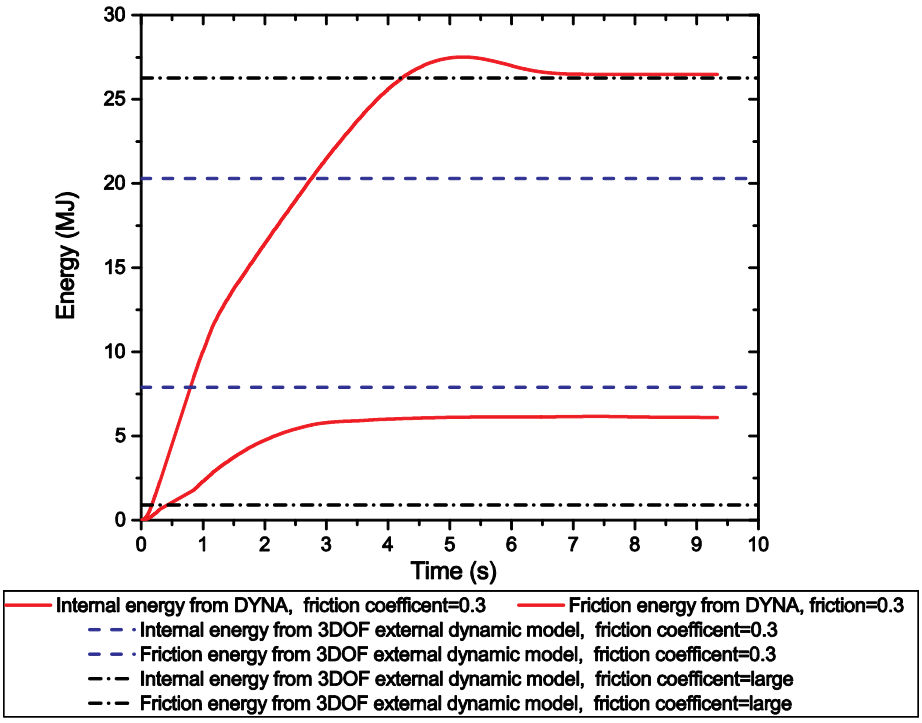

Fig. 27. Internal and friction energy from LS-DYNA and the external dynamic model (scenario 5).

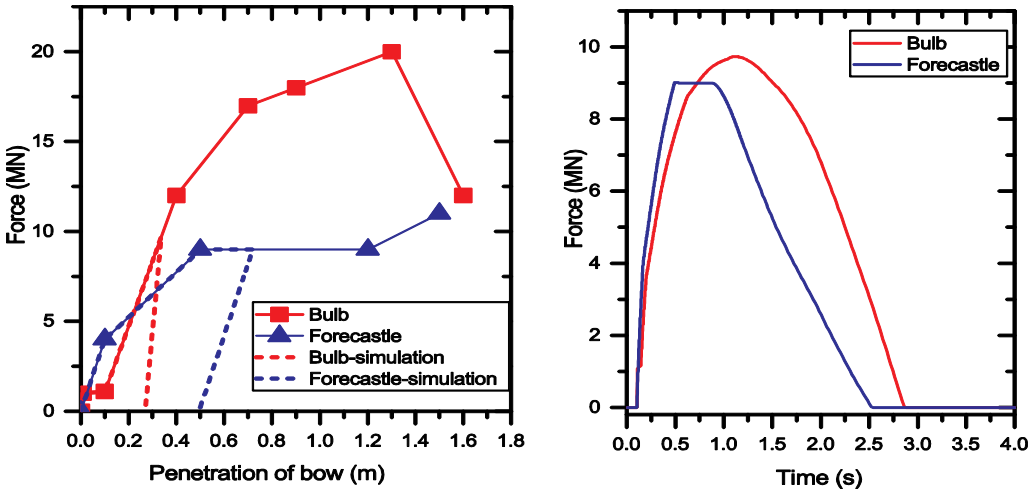

Fig. 28. Contact force versus deformation of bow at forecastle deck and bulb (Left) and force-time histories (Right).

upwards, while the maximum heave displacement at the ship center of gravity is 0.25 m. The sway and yaw motions are indicated by the red trajectory lines in Fig. 26 (a). The time histories of the roll and yaw motions are plotted in Fig. 26 (b). These plots show that the yaw angle is small because, the tube deforms and tends to "wrap" around the ship stem after some time and therefore locks the ship with respect to yaw motion.

The temporal variation of the internal energy and the friction energy is plotted in Fig. 27, and is compared with external dynamic models by Liu and Amdahl (2019). A friction coefficient $\mu = 0.3$ is adopted in the simulation. The plots show that the 3DOF external dynamic model with $\mu = 0.3$ underestimates the energy dissipation, while energy predicted by the 6DOF model is expected to be even lower. This is mainly because, ship motions are locked to some extent due to tube deformations. The collision duration is long with complicated ship trajectories. During the process, the normal vector of the contact surface changes significantly. In this case, the simplified external mechanics models may give inaccurate predictions and yield unconservative results. However, if we give artificially a large friction coefficient to enable a forced sticking case, the predicted internal energy becomes close to simulation results but with smaller friction energy. This indicates that during the external dynamic calculations, the forces in the tangential direction includes not only the friction force but also the tangential deformation resistance, also known as the moving loads. This is consistent with findings in Liu and Amdahl (2019). Additional information regarding assumptions and limitations of the external dynamic models can be found in Yu et al. (2019).

5. Global response simulation in USFOS

Local LS-DYNA analysis with shell modelling gives significant details of structural deformations in the vicinity of the impacted zone. This, however, yields a large number of elements and requires considerable

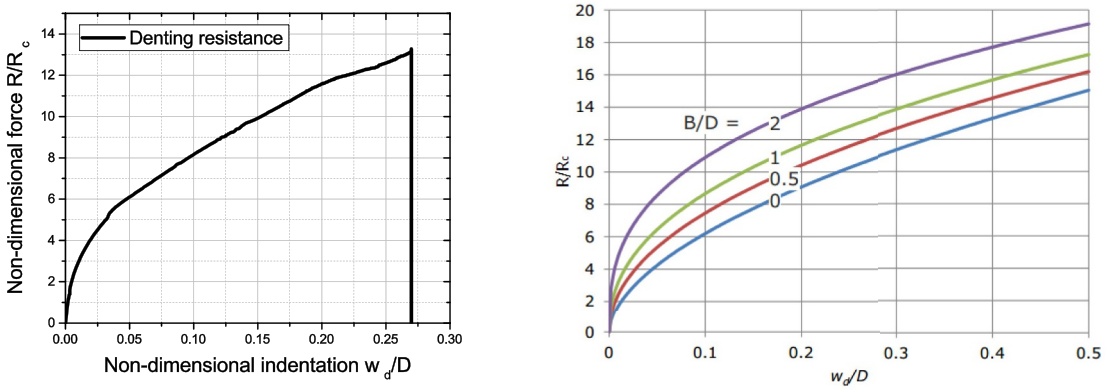

Fig. 29. Non-dimensional force indentation curve for the column subjected to bulb impact. The left figure shows the simulated indentation resistance in USFOS; the right figure is taken from NORSOK-N004 (2004). $R_c = \frac{1}{4}\sigma_y t^2\sqrt{\frac{D}{t}}$, σ_y = yield stress, D = diameter, t = thickness.

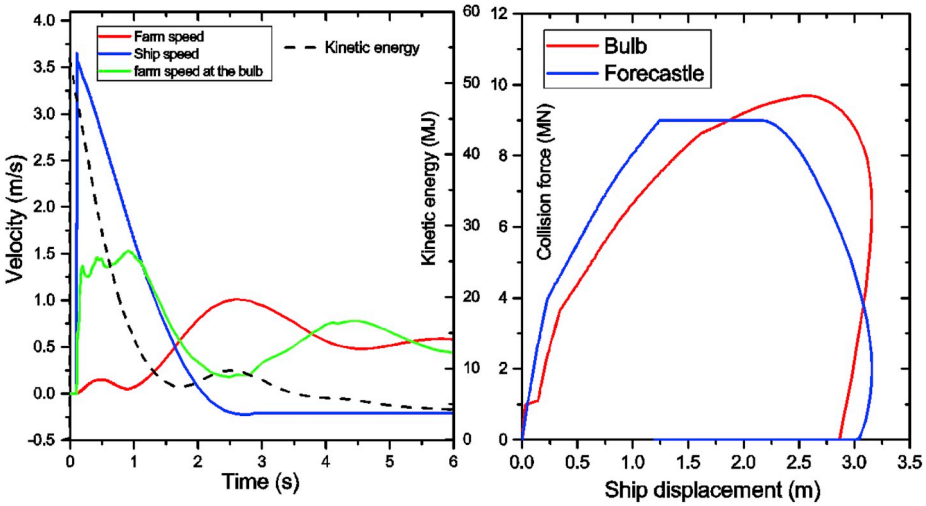

Fig. 30. (left) velocity histories for the ship, the cage center column and the cage at bulb; (right) collision force versus total ship displacement.

computational resources. In addition, the shell model contains only a small part of the fish cage, and the boundaries are fixed in all degrees of freedom. This neglects the interaction between the cage motion and structural deformation. For collision scenarios close to the boundaries, the resulting resistance may be exaggerated, see e.g. scenario 3. In order to verify the boundaries of the local shell model, and to study the global collision response of the fish cage, USFOS is a viable tool with efficient beam formulations and with good accuracy.

The fish cage model used in the USFOS analysis is shown in Fig. 5. It is moored with eight mooring lines. The ring stiffeners are not modeled, but are smeared onto the associated tube. The ship with associated mass (7500 tons displacement plus 10% added mass for head-on collisions in accordance with NORSOK-N003 (2017)) is modeled as a concentrated mass connected to the fish cage model with nonlinear springs; one for the contact with the stem at forecastle deck and one for the contact with the bulb. The force-penetration relationships that are assumed for the bulb and the forecastle are shown in Fig. 28 (left). They are based on information given by Storheim and Amdahl (2014) with the same supply vessel model. The ship was given an initial speed of 3.6 m/s corresponding to a kinetic energy of 53.5 MJ after 0.1 s when the gravity and buoyancy forces have been applied. The good agreement of the input resistance curve and the resistance obtained from simulations indicates correct implementation. Notably, the bulb has a high resistance to deformation. Each deformation spring is connected to an elastic spring that allows the contact to unload completely towards the end of the collision.

The force-time histories from the simulation are plotted in Fig. 28 (right). The peak force at the forecastle deck and at the bulb location is almost equal, but the bulb force has a somewhat longer duration. The actual deformations of the bulb and the forecastle are indicated in Fig. 28 (left). It is noticed that the deformation of the bulb is only 0.3 m, while the stem at forecastle deck undergoes 0.7 m deformation for this force level. Hence, the bulb dissipates only about 1.2 MJ, while the stem at forecastle deck dissipates approximately 4.8 MJ. The diagrams show that the bulb and forecastle have spent a considerable time on the elastic unloading part of the deformation curve, so accurate modelling of unloading may be essential.

While the bulb undergoes very little damage, the vertical column is subjected to a significant local indentation of 0.75 m, approximately 27% of the column diameter, as shown in Fig. 29 (left). The associated denting energy calculated by USFOS is around 4.9 MJ, and is based on the denting curve given in NORSOK-N004 (2004), see Fig. 29 (right). According to NORSOK-N004 (2004), the dent reduces the plastic moment capacity by 60%. This reduction is also realized in the USFOS simulations by creating a plastic hinge at the location of the bulb contact.

From the simulations, the total plastic energy dissipated by the ship and local denting is about 11 MJ at the time of the maximum impact force for the bulb, i.e. after 1.25 s. The fish cage has dissipated 29 MJ energy mainly by structural deformation of the column in the hit area.

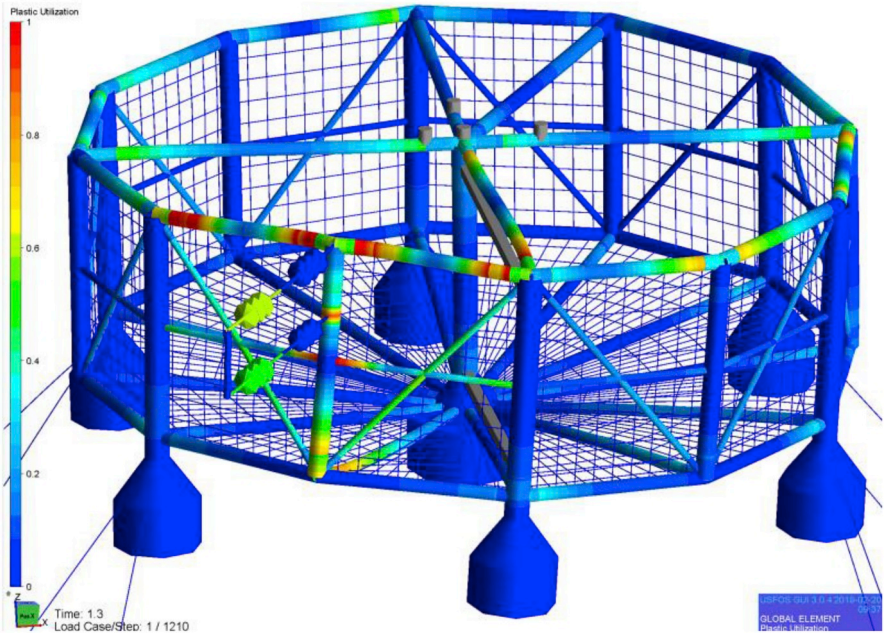

Fig. 31. Deformed configuration of fish cage at maximum collision force (deformations are magnified by 3 times for better illustration).

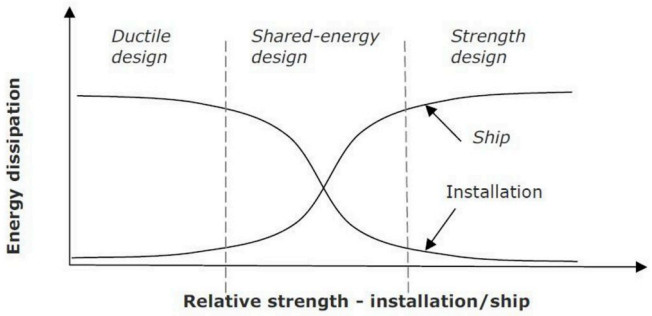

Fig. 32. Energy dissipation for strength, ductile and shared-energy design, from DNV-RP-C204 (2016).

The total kinetic energy has been reduced from 53.5 MJ to 13.5 MJ, where the ship contributes with 7.5 MJ and the kinetic energy of the fish cage is 6 MJ at this stage and is dominated by motion of the hit framework and fish farm rotations while the translational speed of the whole cage is still small (0.15 m/s).

The impulse for the bulb and the forecastle for the entire impact, calculated from the force histories in Fig. 28 (right) amounts to 18.3 MNs and 13 MNs, respectively. Thus, the impulse should give the vessel a change of velocity equal to roughly 3.8 m/s, i.e. the vessel should move with a speed of about 0.2 m/s in the opposite direction after collision. The plot in Fig. 30 (left) confirms this. The mass and added mass of the fish farm is 33400 tons. Hence, the fish farm should get a speed of 1 m/s, which agrees well with the simulated speed at the end of contact. The displacement of the cage center column at the end of collision is virtually zero, and confirms that the impact is highly impulsive. Thus, the local model will provide reliable information of the collision damage.

It is interesting to notice that a simple rigid body model would predict the remaining kinetic energy to be 10.6 MJ at the end of the first impact period (before any partial restitution). This is close to the actual value after 2.8 s in Fig. 30, but it should be recognized that the two bodies do move in opposite direction and not as one body.

The collision forces for the bulb and the forecastle are plotted versus total vessel displacement in Fig. 30 (right). The curves resemble those from local LS-DYNA simulations in Fig. 10. Fig. 31 illustrates the plastic deformations in the fish cage. The overall picture resembles that of the local analysis of scenario 1, most of the damage has been absorbed in the locally modeled region. The supporting columns connected to transverse tubes act as supporting boundaries and their stress states are far from yielding. This shows that it is reasonable to assume clamped conditions at the boundaries. Members outside the direct contact area are seen to be affected to some extent, but the associated energy is negligible compared to the total energy. USFOS predicts that the thin-walled frame at the top center joint undergoes local buckling amounting to approximately 10% of the brace diameter during plastic rotations.

6. Discussion

Local shell analysis and global beam analysis have been used to investigate the structural response of the fish farm cage under supply vessel impacts. As there is no direct design standard for offshore fish farms against ship impacts, established standards and researches for offshore oil and gas may be useful. The design of offshore platforms against ship impacts may be carried out in the ductile, shared-energy or strength design domain (DNV-RP-C204, 2016) (see Fig. 32):

Strength design: The installation is strong enough to resist collision forces with minor deformation, so that the ship is forced to deform and dissipate the major part of the energy.

Ductility design: The installation undergoes large plastic deformation and dissipates the major part of the collision energy.

Shared energy design: Both the installation and the ship contribute significantly to energy dissipation.

From the above local and global analysis, the relative strength of the ship and the offshore fish cage falls predominantly within the ductile design domain, where the fish farm dissipates most of the impact energy through structural deformations. In the design of offshore installations against collisions, structural damage can be allowed provided that it does not impair the main safety functions and does not lead to progressive collapse of the structure or sinking due to puncturing and flooding of buoyancy compartments. Further, the structure should have sufficient residual strength in damaged condition to resist waves and current loads with a certain return period (say 1 year) before it can be

repaired. For fish farms it may also be relevant to introduce a requirement related to net penetration and damage in order to avoid or limit fish escape.

7. Conclusions

This paper presents a combined local and global analysis procedure of supply vessel collisions with an offshore fish farm. The striking ship was selected to be a standard offshore supply vessel with a displacement of 7500 tons. Energy absorption capacity and collapse patterns of the offshore fish farm, and the relative strength of the supply vessel and the fish cage were investigated.

In the local collision analysis, the decoupled simulations show that the fish farm is capable of absorbing considerable energy through structural deformations before complete collapse. In general, the resistance of the fish cage is smaller than that of the striking vessel (especially the bulbous bulb), and most of the impact energy is dissipated by the fish cage. However, the column top with a stiffened plate represents a hard spot of the fish farm, and is capable of crushing the ship stem significantly. The middle column and the transverse tubes are very thin-walled with large diameter/thickness ratios, and are thus susceptible to local buckling and denting. This limits the energy that the tubes can dissipate by plastic bending or by crushing the ship bow.

A single scenario was also analyzed using coupled simulations where ship motions in 6 degrees of freedom were accurately predicted based on potential flow theory for the hydrodynamic loads. The analyses showed the striking ship undergoes significant pitch motions. In addition, the deformed transverse tube is observed to warp around the ship bow and thus constraints further ship motions. External dynamic models do not capture the 'motion locking' effect and predicts lower energy than that from the coupled simulation.

From the global analysis using USFOS, structural damage of the fish cage mainly concentrates on the impacted region, with less damage outside the direct contact area. The analysis confirms the major conclusions for energy absorption and structural damage from the local shell analysis. Possible acceptance criteria for designing offshore fish farms against ship collisions are discussed in view of those adopted for offshore oil and gas structures.

Acknowledgement

This work was supported by the Research Council of Norway through the Centres of Excellence funding scheme, project number 223254 – NTNU AMOS, and through the Centres for Research-Based Innovation funding scheme, project number 237790 – EXPOSED.

Appendix A. Supplementary data

Supplementary data to this article can be found online at https://doi.org/10.1016/j.oceaneng.2019.106653.

References

Alsos, H.S., Amdahl, J., Hopperstad, O.S., 2009. On the resistance to penetration of stiffened plates, Part II: numerical analysis. Int. J. Impact Eng. 36, 875–887.
Amdahl, J., 1980. Impact Capacity of Steel Platforms and Tests on Large Deformations of Tubes and Transverse Loading. Det norske Veritas. Progress Report, 80-0036.
Biehl, F., Lehmann, E., 2006. Collisions of Ships with Offshore Wind Turbines: Calculation and Risk Evaluation. Offshore Wind Energy. Springer.
Bore, P.T., Amdahl, J., 2017. Determination of environmental conditions relevant for the ultimate limit state at an exposed aquaculture location. In: ASME 2017 36th International Conference on Ocean, Offshore and Arctic Engineering. American Society of Mechanical Engineers. V03BT02A043-V03BT02A043.
Cerik, B.C., Shin, H.K., Cho, S.-R., 2015. On the resistance of steel ring-stiffened cylinders subjected to low-velocity mass impact. Int. J. Impact Eng. 84, 108–123.
Cho, S.-R., Lee, H.-S., 2009. Experimental and analytical investigations on the response of stiffened plates subjected to lateral collisions. Mar. Struct. 22, 84–95.
Cockcroft, M., Latham, D., 1968. Ductility and the workability of metals. J. Inst. Met. 96, 33–39.
Costas, M., Morin, D., Hopperstad, O.S., Børvik, T., Langseth, M., 2019. A through-thickness damage regularisation scheme for shell elements subjected to severe bending and membrane deformations. J. Mech. Phys. Solids 123, 190–206.
DNV-RP-C204, 2016. Recommended Practice DNV-RP-C204. DET NORSKE VERITAS.
DNV-RP-C208, 2016. Determination of Structural Capacity by Non-linear FE Analysis Methods. Det Norske Veritas.
Fatt, H., Wierzbicki, T., 1991. Denting analysis of ring stiffened cylindrical shells. Int. J. Offshore Polar Eng. 1.
Firouzsalari, S.E., Showkati, H., Ingham, J.M., 2019. Free-spanning and base-supported tubes subjected to combined axial compression and indentation loads. J. Constr. Steel Res. 161, 341–354.
Hallquist, J.O., 2007. LS-DYNA Keyword User's Manual, vol. 970. Livermore Software Technology Corporation, pp. 1–2.
Kvitrud, A., 2011. Collisions between Platforms and Ships in Norway in the Period 2001-2010. ASME 2011 30th International Conference on Ocean, Offshore and Arctic Engineering. American Society of Mechanical Engineers, pp. 637–641.
Le Sourne, H., Barrera, A., Maliakel, J.B., 2015. Numerical crashworthiness analysis of an offshore wind turbine jacket impacted by a ship. J. Mar. Sci. Technol. 23, 694–704.
Le Sourne, H., Besnard, N., Cheylan, C., Buannic, N., 2012. A ship collision analysis program based on upper bound solutions and coupled with a large rotational ship movement analysis tool. J. Appl. Math. 2012, 27.
Le Sourne, H., Pire, T., Hsieh, J.R., Rigo, P., 2016. New analytical developments to study local and global deformations of an offshore wind turbine jacket impacted by a ship. In: Proceedings of the 7th International Conference on Collision and Grounding of Ships and Offshore Structures (ICCGS2016), Ulsan, South Korea.
Liu, Z., Amdahl, J., 2019. On multi-planar impact mechanics in ship collisions. Mar. Struct. 63, 364–383.
Marinatos, J., Samuelides, M., 2015. Towards a unified methodology for the simulation of rupture in collision and grounding of ships. Mar. Struct. 42, 1–32.
Marintek, 2012. Simo - user's manual Version 4.0 rev0. Marintek Report.
Minorsky, V., 1958. An Analysis of Ship Collisions with Reference to Protection of Nuclear Power Plants. Sharp (George G.) Inc., New York.
Moan, T., Amdahl, J., Gerhard, E., 2017. Assessment of ship impact risk to offshore structures-new NORSOK N-003 guidelines. Mar. Struct. 63, 480–494.
Noh, M.-H., Cerik, B.C., Han, D., Choung, J., 2018. Lateral impact tests on FH32 grade steel stiffened plates at room and sub-zero temperatures. Int. J. Impact Eng. 115, 36–47.
NORSOK-N003, 2017. 2017. NORSOK Standard N-003.
NORSOK-N004, 2004. Design of steel structures. Rev.
Ohtsubo, H., Kawamoto, Y., Kuroiwa, T., 1994. Experimental and numerical research on ship collision and grounding of oil tankers. Nucl. Eng. Des. 150, 385–396.
Paik, J., 2007. Practical techniques for finite element modelling to simulate structural crashworthiness in ship collisions and grounding (Part II: verification). Ships Offshore Struct. 2, 81–85.
Pedersen, P.T., Zhang, S., 1998. On impact mechanics in ship collisions. Mar. Struct. 11, 429–449.
Peschmann, J., 2001. Energy Absorption Computations of Ship Steel Structures under Collision and Grounding (Translated from German Language). Schriftenreihe Schiffbau/TU Hamburg-Harburg, p. 613.
Petersen, M.J., 1982. Dynamics of ship collisions. Ocean. Eng. 9, 295–329.
Pill, I., Tabri, K., 2011. Finite element simulations of ship collisions: a coupled approach to external dynamics and inner mechanics. Ships Offshore Struct. 6, 59–66.
Pire, T., Le Sourne, H., Echeverry, S., Rigo, P., 2018. Analytical formulations to assess the energy dissipated at the base of an offshore wind turbine jacket impacted by a ship. Mar. Struct. 59, 192–218.
Qu, H., Huo, J., Li, A., Jiang, Y., Liu, Y., 2017. Experimental study on impact behaviour of steel plane tubular frames. Thin-Walled Struct. 111, 210–223.
Rice, J.R., Tracey, D.M., 1969. On the ductile enlargement of voids in triaxial stress fields*. J. Mech. Phys. Solids 17, 201–217.
Samuelides, E., Frieze, P., 1989. Fluid-structure interaction in ship collisions. Mar. Struct. 2, 65–88.
Sha, Y., Amdahl, J., Dørum, C., 2019. Local and global responses of a floating bridge under ship–girder collisions. J. Offshore Mech. Arct. Eng. 141, 031601.
Simonsen, B.C., Törnqvist, R., 2004. Experimental and numerical modelling of ductile crack propagation in large-scale shell structures. Mar. Struct. 17, 1–27.
Soreide, T., Amdahl, J., Eberg, E., Hellan, O., Halmås, T., 1999. USFOS–a Computer Program for Progressive Collapse Analysis of Steel Offshore Structures. Theory Manual. SINTEF Report STF71 F, p. 88038.
Standard-Norway-NS9415, 2009. Norway-Standard, Marine Fish Farms-Requirements for Site Survey, Risk Analyses, Design, Dimensioning, Production, Installation and Operation. NS9415.
Storheim, M., 2016. Structural Response in Ship-Platform and Ship-Ice Collisions.
Storheim, M., Amdahl, J., 2014. Design of offshore structures against accidental ship collisions. Mar. Struct. 37, 135–172.
Storheim, M., Amdahl, J., Martens, I., 2015. On the accuracy of fracture estimation in collision analysis of ship and offshore structures. Mar. Struct. 44, 254–287.
Tabri, K., Varsta, P., Matusiak, J., 2010. Numerical and experimental motion simulations of nonsymmetric ship collisions. J. Mar. Sci. Technol. 15, 87–101.
Tautz, I., Schöttelndreyer, M., Lehmann, E., Fricke, W., 2013. Collision tests with rigid and deformable bulbous bows driven against double hull side structures. In: 6th International Conference on Collision and Grounding of Ships and Offshore Structures. ICCGS, pp. 93–100.
Travanca, J., Hao, H., 2015. Energy dissipation in high-energy ship-offshore jacket platform collisions. Mar. Struct. 40, 1–37.
Tørnqvist, R., 2003. Design of Crashworthy Ship Structures. Technical University of Denmark, Kgns Lyngby, Denmark.

Wang, Z., Liu, K., Ji, C., Chen, D., Wang, G., Soares, C.G., 2016. Experimental and numerical investigations on the T joint of jack-up platform laterally punched by a knife edge indenter. Ocean. Eng. 127, 212–225.
Wierzbicki, T., Suh, M., 1988. Indentation of tubes under combined loading. Int. J. Mech. Sci. 30, 229–248.
Yu, Z., Amdahl, J., 2018. Analysis and design of offshore tubular members against ship impacts. Mar. Struct. 58, 109–135.
Yu, Z., Amdahl, J., 2018. A review of structural responses and design of offshore tubular structures subjected to ship impacts. Ocean. Eng. 154, 177–203.
Yu, Z., Liu, Z., Amdahl, J., 2019. Discussion of assumptions behind the external dynamic models in ship collisions and groundings. Ships Offshore Struct.
Yu, Z., Shen, Y., Amdahl, J., Greco, M., 2016. Implementation of linear potential-flow theory in the 6DOF coupled simulation of ship collision and grounding accidents. J. Ship Res. 60, 119–144.
Zhu, L., Liu, Q., Jones, N., Chen, M., 2017. Experimental study on the deformation of fully clamped pipes under lateral impact. Int. J. Impact Eng. 111, 94–105.